Observation of an Accidental Bound State in the Continuum in a Chain of Dielectric Disks

M.S. Sidorenko,[1,][*] O.N. Sergaeva[,][1] Z.F. Sadrieva[,][1] C. Roques-Carmes[,][2] P.S. Muraev,[3,4] D.N. Maksimov,[3,4] and A.A. Bogdanov[1,][†]

[1]*Department of Physics and Engineering, ITMO University, St. Petersburg 197101, Russia*

[2]*Research Laboratory of Electronics, Massachusetts Institute of Technology, 50 Vassar Street, Cambridge, Massachusetts USA*

[3]*Kirensky Institute of Physics, Federal Research Center KSC SB RAS, Krasnoyarsk 660036, Russia*

[4]*Siberian Federal University, Krasnoyarsk 660041, Russia*

Being a general wave phenomenon, bound states in the continuum (BICs) appear in acoustic, hydrodynamic, and photonic systems of various dimensionalities. Here, we report the first experimental observation of an accidental electromagnetic BIC in a one-dimensional periodic chain of coaxial ceramic disks. We show that the accidental BIC manifests itself as a narrow peak in the transmission spectra of the chain placed between two loop antennas. We demonstrate a linear growth of the radiative quality factor of the BICs with the number of disks that is well described with the developed tight-binding model. We estimate the number of disks when the radiation losses become negligible in comparison to material absorption and, therefore, the chain can be considered as practically infinite. The presented analysis is supported by near-field measurements of the BIC profile. The obtained results provide useful guidelines for practical implementations of structures with BICs opening up horizons for the development of radio-frequency and optical metadevices.

I. INTRODUCTION

Dielectric resonators are open systems whose eigenmodes couple to the radiation continuum. Because of the coupling, the eigenmodes are generally expected to have finite lifetimes because of radiation losses. For a long time, it was believed that only guided modes with frequencies below the light line were decoupled from the radiation continuum [1,2]. Nevertheless, in the early 2000s, several counterexamples of perfectly localized states—i.e., totally decoupled from the radiation continuum—at frequencies above the light line were proposed in dielectric gratings and photonic crystal waveguides [3–5]. Historically, a similar phenomenon was first predicted for quantum particles trapped above quantum-well barriers [6]. Such localized states are known as *bound states in the continuum* (BICs).

A genuine BIC having an infinite radiative quality factor (*Q* factor) is a mathematical idealization. Its practical implementation is possible only in infinite periodic systems [7] or in finite systems with exploiting perfect conducting walls or epsilon-near-zero materials [8].

In practice, one can only observe a quasi-BIC with finite *Q* factor. The *Q* factor is limited due to several factors such as the finite size of the resonator [9–12], structure imperfections [13,14], influence of the substrate [15,16], surface roughness [16], symmetry breaking [15,17], and material losses [9,16,18]. Recent progress in photonic crystals fabrication and characterization stimulated extensive studies of BICs in various periodic photonic structures with potential applications to lasing sources [19,20], fiber Bragg gratings [21,22], sensing [23–26], optical filtering [27–29], enhanced light-matter interaction [30–35], nonlinear nano-optics [26,36,37], spintronics [38], and optical vortex generation [39,40].

Among the variety of available periodic photonic systems, a one-dimensional array of spheres or disks stands out because of its rotational symmetry. This gives rise to BICs with nontrivial orbital angular momentum (OAM) [41,42]. Such states could be used to generate vortex beams [39,40] with potential applications in optomechanics [43] and quantum cryptography [44]. The theory of a BIC with OAM was developed in Refs. [45–47]. The experimental observation of a symmetry-protected BIC with zero OAM was reported in Ref. [9] in the gigahertz frequency range and then shortly after in the visible range [21]. So far, all experimentally reported BICs

_____

[*]mikhail.sidorenko@metalab.ifmo.ru
[†]a.bogdanov@metalab.ifmo.ru

in one-dimensional arrays fell into the category of in-Γ (symmetry-protected) BICs. Such BICs are standing waves that do not couple with outgoing radiative waves due to symmetry.

In this work, we focus on off-Γ (accidental) BICs that are traveling Bloch waves propagating along the ceramic disks chain [15]. While the in-Γ BICs are insensitive to variation of the system's parameters, the experimental detection of an accidental BIC is more challenging, since it requires fine adjustment of the system's parameters, namely, radius, height of the disks, period, or permittivity. We analyze the transformation of a resonant state into an accidental BIC with zero OAM in an axially symmetric one-dimensional (1D) periodic array of dielectric disk resonators. We experimentally demonstrate this transformation in the gigahertz frequency range by increasing the number of chain periods.

The paper is organized as follows. In Sec. II we discuss the eigenmode spectrum of the infinite chain with both in-Γ and off-Γ BICs. In Sec. III we turn to the realistic chain of a finite length and discuss the transformation of high-Q resonances to a BIC as the number of disks increases. We also introduce a tight-binding model that well describes this transformation. Section IV contains the experimental results confirming the theoretical predictions. In Appendix A, we provide the detailed description of the

sample. In Appendix B, we discuss the coupling efficiency of the sample to the loop antennas.

II. INFINITE CHAIN—THEORY

First, we consider the infinite periodic chain of ceramic disks shown in Fig. 1(a). Applying Bloch's theorem and taking into account the axial rotational symmetry of the system, the electric field of an eigenmode can be written as

$$\mathbf{E}(r,\varphi,z,t) = \mathbf{U}_{m,k_z}(r,z)e^{-i\omega t \pm ik_z z \pm im\varphi}, \quad (1)$$

where k_z is the Bloch wave vector defined in the first Brillouin zone, m (an integer number) is the OAM, and $\mathbf{U}_{m,k_z}(r,z)$ is the periodic Bloch amplitude. Because of the reflection symmetry $z \to -z$, the eigenmodes propagating in the $+z$ and $-z$ directions are degenerate, which results in the $\pm$ sign in the argument of the exponential. Since the function $\mathbf{U}_{m,k_z}(z,r)$ is periodic in z with period L, it can be expanded in a Fourier series as

$$\mathbf{U}_{m,k_z}(r,z) = \sum_n \mathbf{C}_{m,k_z}^n(r)\, e^{2\pi inz/L}, \quad (2a)$$

where

$$\mathbf{C}_{m,k_z}^n(r) = \frac{1}{L}\int_{-L/2}^{L/2} \mathbf{U}_{m,k_z}(r,z)\, e^{-2\pi inz/L}dz. \quad (2b)$$
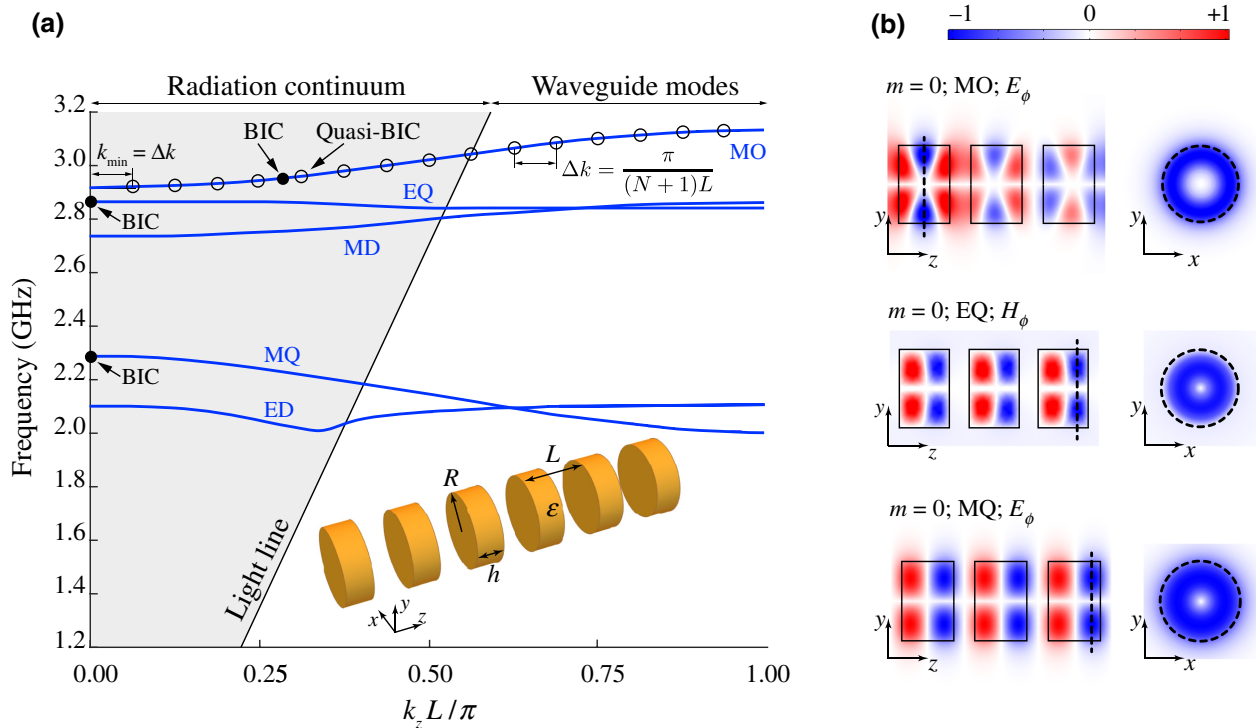

FIG. 1. Bound states in the continuum in the chain of ceramic disks with period $L = 28$ mm, radius $R = 15$ mm, height $h = 20$ mm, and permittivity $\varepsilon = 44$. (a) Photonic band structure of an infinite chain of disks with symmetry-protected and accidental BICs. Several modes with zero OAM $m = 0$ are shown: ED, MD, EQ, MQ, MO The inset shows a 3D rendering of the chain. (b) Side and front views of the field distribution for the BICs.

The index n is an integer and it corresponds to the diffraction order. Generally, the Fourier coefficient $\mathbf{C}_{m,k_z}^n(r)$ defines the amplitude of the near-field or outgoing wave carrying energy away from the structure. In the subwavelength regime $L < \lambda$, only the zeroth diffraction order ($n = 0$) is nonzero.

In Fig. 1(a) we show the dispersion of the modes with $m = 0$. The simulation is performed for the chain with period $L = 28$ mm composed of disks with diameter $D = 30$ mm, height $h = 20$ mm, and permittivity $\varepsilon = 44$. The gray area depicts the domain where only the zeroth diffraction order is open. Thus, if $k_z < \omega/c < |k_z \pm 2\pi/L|$, the radiation losses are determined by the zero-order Fourier coefficient only. If the zero-order Fourier amplitude $\mathbf{C}_{m,k_z}^0(r)$ equates to zero, the leaky resonant eigenmode turns into a BIC [15]. By definition, the zero-order Fourier coefficient is the spatial average of the electric field over a period. The center of the Brillouin zone is the Γ point, where the symmetry of the field distribution follows the point symmetry of the chain, i.e., modes transform by the irreducible representations of the chain's point-group symmetry [48,49]. Since the chain is invariant under reflection in the plane $z = 0$, the modes are divided into odd and even with respect to the $z \rightarrow -z$ transformation. Obviously, the integration of an odd function $\mathbf{U}_{m,k_z}(r, z)$ with respect to z yields zero coupling. In this case, we observe a symmetry-protected BIC with the coupling to the radiation continuum prevented by the point symmetry of the chain.

In Fig. 1(b), we show that the odd modes are formed by the electric quadrupole (EQ) and magnetic quadrupole (MQ) Mie resonances whose directivity patterns are the xy-nodal surface. Therefore, these modes do not contribute to the far field in the direction of a single open diffraction channel coinciding with the y axis. In contrast, the even modes such as the magnetic octupole (MO), magnetic dipole (MD), and electric dipole (ED) radiate in the y direction. The dispersion of the radiation losses of MD, EQ, and MO modes characterized by $\gamma = \mathrm{Im}[\omega(k_z)]$ is shown in Fig. 2(a). While γ remains constant for the MD mode, the radiation loss of the EQ mode limits to zero as k_z^2 in the vicinity of the Γ point, revealing the emergence of a symmetry-protected BIC.

The Fourier coefficient corresponding to the open diffraction channel [Eq. (2b)] can vanish even if $\mathbf{U}_{m,k_z}(r, z)$ is a noneven function of z. Moreover, it is possible at an arbitrary point k_z by tuning the parameters of the chain. A BIC appearing in this case is called an off-Γ BIC, a *tunable* BIC, or an *accidental* BIC [50]. The term "accidental" does not mean that the BIC appeared by accident, it just highlights that it is difficult to predict the position of such a BIC in the parametric space in advance. For instance, the MO mode turns to the accidental BIC at the specific k_z whose field distribution is shown in Fig. 1(b). The leakage vanishes when all multipoles forming the mode interfere destructively in the direction of the open diffraction channel [51]. The accidental BIC on the MO dispersion branch manifests itself in the vanishing of the radiative losses, as shown in Fig. 2(a).

It is known that the states with nonzero OAM ($m \neq 0$) exhibit hybrid polarization, while modes with $m = 0$ can be divided into transverse electric (TE) and transverse magnetic (TM) [52,53]. Hereinafter, TE (respectively TM) refers to a field decomposition of the form $\mathbf{E} = (0, E_\varphi, 0)$ and $\mathbf{H} = (H_r, 0, H_z)$ [respectively $\mathbf{E} = (E_r, 0, E_z)$ and $\mathbf{H} = (0, H_\varphi, 0)$]. For a hybrid polarization
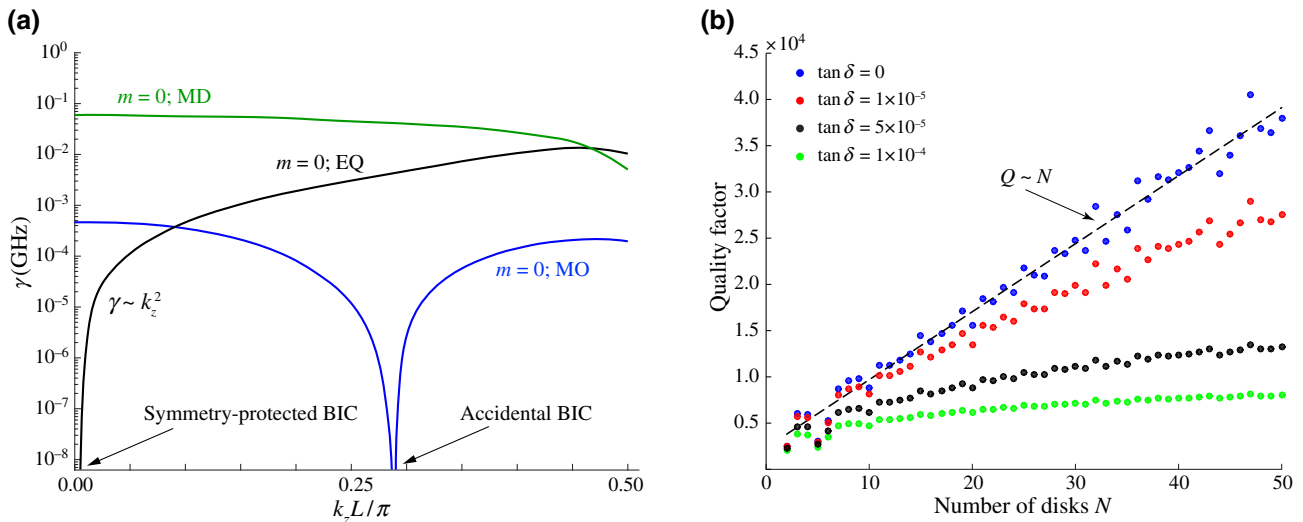

FIG. 2.   (a) Radiation losses of three selected modes in the infinite chain found numerically. (b) Dependence of the Q factor of the accidental quasi-BIC as a function of the number of disks for different levels of material losses.

$C_{\text{TE}} \cdot (H_r, E_\varphi, H_z) + C_{\text{TM}} \cdot (H_r, H_\varphi, E_z)$, an additional degree of freedom $C_{\text{TE(TM)}}$ arises in the system.

As long as for the particular polarization the parity of the $E_{(\cdot)}$ and $H_{(\cdot)}$ components are opposite, it is impossible to obtain a zero spatial average of the electric and magnetic field components simultaneously [53]. Therefore, a symmetry-protected BIC with nonzero OAM does not exist. However, an accidental BIC can be obtained by tuning the geometrical and material parameters of the structure.

III. FINITE CHAIN—THEORY

A. Fabry-Perot quantization

In experiments, we always deal with structures of finite sizes. In this case, the ends of the chain play the role of partially reflecting mirrors and, thus, the chain can be considered as a Fabry-Perot resonator. The continued frequency band of the infinite chain is quantized into Fabry-Perot resonances with finite Q factors limited by the scattering from the ends of the chain. Therefore, in a finite chain, a genuine BIC turns into a quasi-BIC with a finite Q factor.

For the chain of N scatterers, the continuous band of the infinite chain is replaced by a finite set of N Fabry-Perot resonances at frequencies $\omega(k_z)$ corresponding to the quantized quasiwave vector $k_z = p\pi/[(N+1)L]$, where p is an integer and L is the period. The highest Q-factor resonant state has the quantized wave vector closest to the BIC (observed in the infinite periodic system) and, thus, can be associated with the quasi-BIC [see Fig. 1(a)]. Similarly, a symmetry-protected quasi-BIC coincides with the first resonant state related to the minimal wave vector $k_z = \pi/[(N+1)L]$, as we showed in Ref. [9]. In the case of an off-Γ BIC, though, the index p of the nearest to BIC resonance changes as the number of disks increases. The change in p also explains the fluctuation of the Q factor around the mean; the distance in the k space between genuine BIC and the quasi-BIC can take arbitrary values in the interval $[-\pi/\{2(N+1)L\}, \pi/\{2(N+1)L\}]$.

Our simulations show that the Q factor of the resonant state associated with the accidental out-of-Γ quasi-BIC can be approximated by a linear function of the number of disks N; see Fig. 2(b). The experimental study of this dependence is provided in Sec. IV. Here, we highlight that the Q factor of a symmetry-protected quasi-BIC grows as N^2 [9,12]. In contrast, the Q factor of an accidental quasi-BIC at the Γ point scales as N^3 with the number of disks [12,54]. To explain the difference in the asymptotic behavior of the Q factor, we introduce a simple tight-binding model that accounts for partial reflections from the ends of the chain. Using the tight-binding model is quite natural as the disks are made of high-refractive-index ceramic disks tightly trapping the Mie modes inside [see Fig. 1(b)].

B. Tight-binding model

In a finite chain, the propagating Bloch solutions reflect from the ends of the chain, forming Fabry-Perot resonances—standing waves with a quantized propagation constant k_z. As we are interested only in the behavior in the vicinity of the accidental BIC, we only account for the radiation losses at the ends of the chain, neglecting losses due to detuning from the BIC point. Mathematically, the system described above can be formulated as the eigenvalue problem

$$(\widehat{H}_{\text{eff}} - \omega)|\psi\rangle = 0, \quad (3)$$

where $\widehat{H}_{\text{eff}}$ is a non-Hermitian operator describing both wave propagation between the mirrors and radiation losses when reflecting from the edges of the array. Equation (3) can be introduced by projecting the full-wave Maxwell equation onto the Wannier states of the guided modes. Thus, the amplitude of the electromagnetic field at the qth site is given by

$$\psi(q) = \langle q|\psi\rangle, \quad (4)$$

where $|q\rangle$ is the Wannier function localized at this site. The operator $\widehat{H}_{\text{eff}}$ can be defined by its action on the array of the local field amplitudes

$$-\frac{1}{2}\begin{pmatrix} i\eta & J & \dots & 0 \\ J & 0 & \dots & 0 \\ \vdots & \vdots & \ddots & \vdots \\ 0 & 0 & \dots & i\eta \end{pmatrix}\begin{pmatrix} \psi(1) \\ \psi(2) \\ \vdots \\ \psi(N) \end{pmatrix} = \omega\begin{pmatrix} \psi(1) \\ \psi(2) \\ \vdots \\ \psi(N) \end{pmatrix}, \quad (5)$$

where J describes the optical coupling between the sites (disks) and η accounts for the radiation losses in reflection from the edges. For simplicity, we only introduce nearest-neighbor couplings in Eq. (5). Based on our numerical findings we can conclude that $\eta \ll J$.

Let us look for the radiative eigenmode in the form of a superposition of two counterpropagating waves

$$\psi(q) = Ae^{ikq} + Be^{-ikq} \quad (6)$$

with dispersion

$$\omega = -J\cos(k). \quad (7)$$

After substituting Eq. (6) into Eq. (5) one finds that k satisfies the equation

$$\sin[k(N+1)] - 2i\frac{\eta}{J}\sin[kN] - \left(\frac{\eta}{J}\right)^2\sin[k(N-1)] = 0. \quad (8)$$

Let us introduce a series expansion of k in the powers of η/J, i.e.,

$$k = k_p^{(0)}(N) + \alpha_p(N)\frac{\eta}{J} + \mathcal{O}\left[\left(\frac{\eta}{J}\right)^2\right], \qquad (9)$$

where

$$k_p^{(0)}(N) = \frac{\pi p}{N+1}, \qquad p = 1, 2, \ldots, N, \qquad (10)$$

is the zeroth-order solution corresponding to the lossless chain and $\alpha_p(N)$ gives the correction to the wavevector in the first perturbation order. After substituting Eq. (9) into Eq. (8) and collecting the terms of the same order in η/J, we find that

$$\alpha_p(N) = 2i(-1)^p \frac{\sin[k_p^{(0)}(N)]}{N+1}. \qquad (11)$$

Note that $\alpha_p(N)$ is imaginary since it is solely due to the radiative losses. Finally, the inverse lifetime $\gamma_p = \mathrm{Im}\{\omega_p\}$ is found by substituting Eq. (9) into Eq. (7) to obtain

$$\gamma_p = \frac{\eta}{N+1} \sin^2[k_p^{(0)}(N)]. \qquad (12)$$

One can evaluate the Q-factor scaling law against N by examining the asymptotics of Eq. (12). For an in-Γ resonant state, we take $p = 1$ and $k_1^{(0)}(N) = \pi/(NL)$. Thus, it follows from Eq. (12) that $\gamma_1 \propto 1/N^3$, which is in accordance with previous findings by Blaustein *et al.* [11]. In the case of an off-Γ resonant state, however, we have to keep $k_p^{(0)}(N)$ fixed. Then, Eq. (12) yields

$$\gamma \propto 1/N. \qquad (13)$$

Note that we do not use a subscript in the above equation as the resonances with the wave number nearest to given k_z always have a different number p.

As mentioned above, our model neglects the radiation losses due to k_z detuning. Generally, the total losses of a Fabry-Perot resonance in the chain are comprised of radiation at the ends of the chain and of side radiation existing due to the leaky nature of the propagation band. The total radiative Q factor, Q_{rad} is then given by

$$Q_{\mathrm{rad}} = \frac{Q_1 Q_2}{Q_1 + Q_2}, \qquad (14)$$

where Q_1 is due to the radiation at the edges, while Q_2 accounts for radiation by the leaky band itself. Note that Q_2 is also a diverging quantity as the BIC point is separated from the nearest resonance by a distance of less than

$\pi/(2NL)$, as seen from Fig. 1(a). Then, for Q_2, we have

$$Q_2 \propto N^2, \qquad (15)$$

since the dispersion of the radiation rate must be quadratic in the spectral vicinity of a BIC because the radiation rate is non-negative. Therefore, with $N \to \infty$ we have

$$Q_{\mathrm{rad}} \propto N. \qquad (16)$$

We mention in passing that the dispersion of the radiation rate in the vicinity of an in-Γ accidental BIC is quartic [55,56]. Then, according to Eq. (14), the edge losses dominate in the asymptotic behavior and we have $Q_{\mathrm{rad}} \propto N^3$, as shown in Ref. [12].

C. Material losses

Besides the radiation losses due to the finite size of the chain, there are other sources of losses (absorption in material, roughness of the scatterers, structural disorder, leakage into the substrate, etc.) that contribute to the total losses even for an infinite chain [13,16,18]. In our case, the loss mechanism limiting the total Q factor for a large number of disks ($N \gg 1$) is absorption in the ceramics. Therefore, the total Q factor (Q_{tot}) can be found as

$$Q_{\mathrm{tot}}^{-1} = Q_{\mathrm{rad}}^{-1} + Q_{\mathrm{abs}}^{-1}, \qquad (17)$$

where $Q_{\mathrm{abs}} \approx 1/\tan\delta = \mathrm{Re}(\varepsilon)/\mathrm{Im}(\varepsilon)$.

In Fig. 2(b) we show the dependence of the Q_{tot} factor of the quasi-BIC on the number of disks N for various $\tan\delta$—tangent of material losses. For a large number of disks, Q_{tot} saturates, i.e., the material losses give the major contribution to the total losses. Practically, we can determine how many disks in the chain are necessary to neglect finite-size effects with respect to other sources of losses. This issue is discussed in the next section.

IV. EXPERIMENTAL DEMONSTRATION

A. Transmission measurement

We consider a chain of at most 48 disks with period $L = 28$ mm, where each disk is made of a ceramic material with $\varepsilon = 44$ and $\tan\delta = 1 \times 10^{-4}$ with dimensions $D = 30$ mm and $h = 20$ mm (for more details, see Appendix A). As mentioned in Sec. II, the two polarization components of a mode with $m = 0$ can be distinguished completely. Therefore, TE and TM modes can be excited separately by magnetic or electric dipole antennas, respectively. We excite the magnetic octupole (TE) mode via near-field coupling with a magnetic dipole antenna. Two shielded loop antennas are placed along the same axis at 5 mm distances from the corresponding faces of the first and last cylinders of the chain. The resonant frequencies of each antenna are higher than the frequency band of interest.
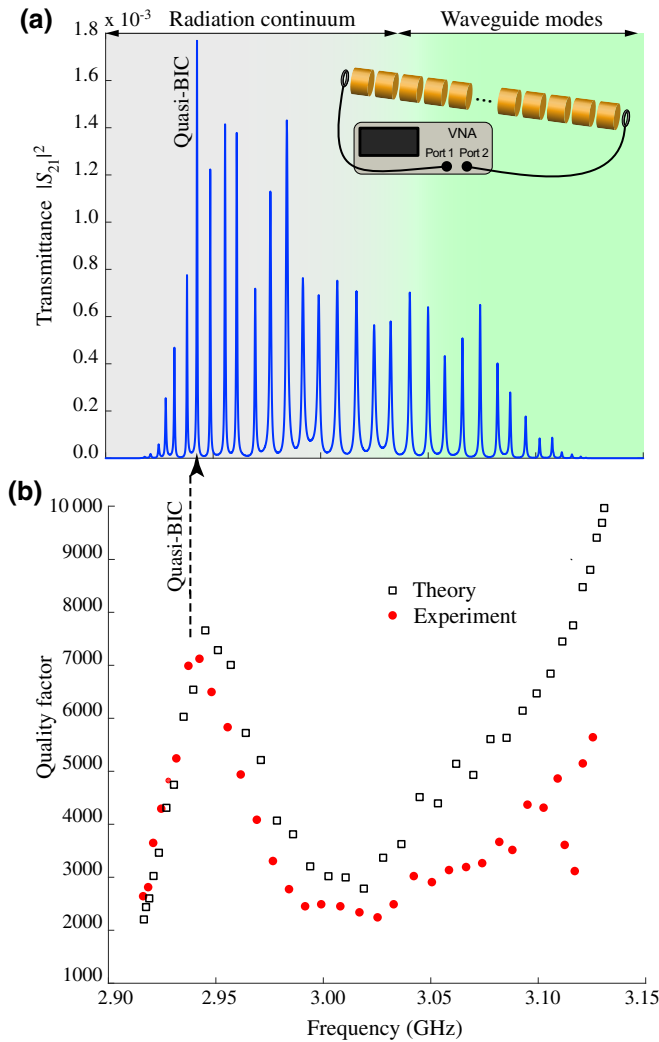
FIG. 3. (a) Transmission spectrum of the 38-disk chain. The magnetic octupole (TE) mode with $m = 0$ is excited with an electric dipole antenna. The green shaded area represents the frequency domain of waveguide modes, while the gray shaded area the represents the radiation continuum. The inset shows the experimental setup for transmission spectrum measurements. (b) The Q factor of the resonant states of the chain composed of the 38 disks. The accidental quasi-BIC is observed at a frequency of about 2.94 GHz.

Such antenna placement allows us to assume weak coupling, which makes the analysis of the Q factor eligible. The scheme of the transmission spectrum measurement setup is provided in Fig. 3(a). Both antennas are connected to the corresponding ports of a vector network analyser (VNA) from Rohde & Schwarz. The transmission spectrum is measured as the S_{21} parameter from the VNA. The measured frequency band is from 2.9 to 3.15 GHz, with 3.2×10^4 frequency samples taken in this interval. This large number of frequency samples ensures sufficient resolution to carefully observe high-Q modes in the transmission spectrum.
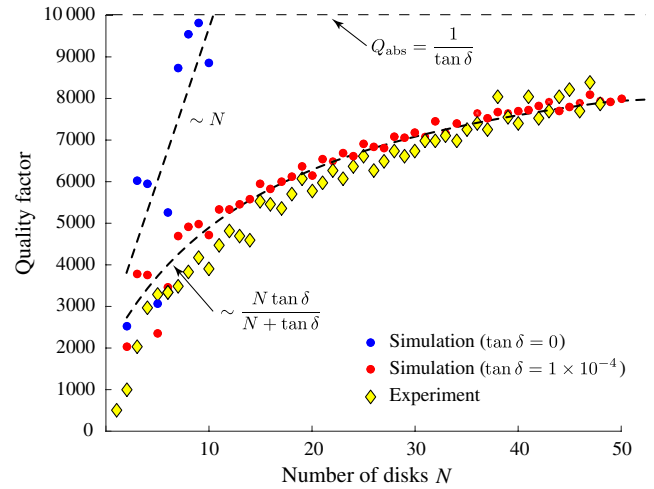

FIG. 4. Experimental and theoretical dependencies of the Q factor of the accidental quasi-BIC. The dashed line corresponds to the predicted scaling lax for the lossless disk chain.

A sample of a measured transmission spectrum for the chain of 38 cylinders is plotted in Fig. 3(a). The resonances lying in the green area correspond to the waveguide modes, those in the gray area are leaky modes coupled to the radiation continuum.

The loaded Q factor is then extracted as $Q_{\text{loaded}} = f_0/2\Delta f$, where Δf is the half-width of the transmission spectrum local maximum at frequency f_0. The width is measured at the level 0.7 of the local maximum value. The measured values of the loaded Q factor for a 38-disk chain are plotted as a function of resonant frequency in Fig. 3(b). On the same plot, a theoretical curve for the Q-factor values is also presented, obtained from the theory developed in Secs. II and III. The sharpest peak in the transmission spectrum corresponds to the accidental quasi-BIC. The sufficiently high intensity of the quasi-BIC indicates that it couples efficiently to the loop antennas placed at the end of the chain (see Appendix B). Moreover, the theoretical curve in Fig. 3(b) (dotted line) shows that structural disorder has a negligible effect. Despite the leakage and absorption, we clearly observe the maximum in Q versus frequency, indicating the manifestation of an accidental BIC.

Then, we measure the transmission spectra for the chain consisting of a different number of disks N and extract the value of the Q factor corresponding to the accidental quasi-BIC. The resulting experimental dependence Q versus N is shown in Fig. 4. The experimental curve fits the theoretical curve very well; see Eq. (17). Although the theory predicts the linear dependence of the Q factor on the number of disks expressed by Eq. (16), the material losses result in an essential deviation from the $Q \sim N$ law. When increasing the number of disks, the total Q_{tot} factor saturates at $Q_{\text{abs}} = 1/\tan\delta$. With smaller material
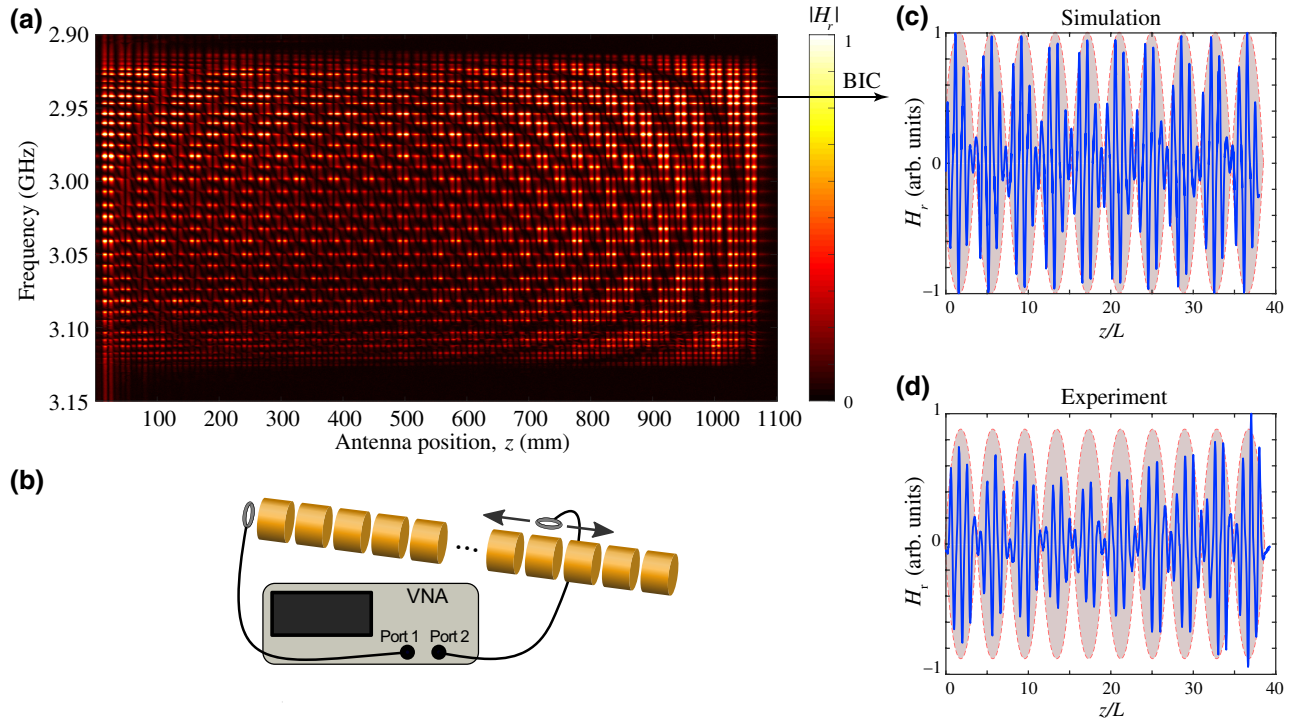
FIG. 5.   (a) Measured radial component of the magnetic field as a function of the antenna position z and frequency. The antenna is moved along the chain. (b) Experimental setup for the measurement of the radial component of the magnetic field. Panels (c),(d) show magnetic field distributions obtained from simulation and experiment at the frequency of the BIC.

losses, one could achieve a larger Q factor in the limit of long chains. The analyzed chain of ceramics disks is characterized by $\tan\delta = 1 \times 10^{-4}$. Therefore, the saturation level $Q_{abs} = 10^4$ shows the maximal Q_{tot} factor that can be obtained for the infinitely long chain.

One can see that, for N more than about 30, the total Q factor of the quasi-BIC saturates with the number of disks, and the chain can be considered as practically infinite. Therefore, for a greater number of periods, the quasi-BIC is almost indistinguishable from a genuine BIC in the infinite chain.

An interesting feature of the measured transmission spectrum is that the transmission is minimal at the edges of the frequency band, namely, for the leaky mode near the Γ point ($\nu = 2.92$ GHz) and waveguide mode near the band edge ($\nu = 3.13$ GHz). This is explained by the weak overlap of these modes with the loop antennas (see Appendix B for details).

B. Field distribution measurements

We also measure the spatial and spectral distributions of the radial component of the magnetic field along the chain of cylinders measured. The measurements are performed in the near field using a magnetic loop antenna with the main axis coinciding with the cylinder radius [see Fig. 5(b)]. The distance between the antenna and the cylinder wall is 2 mm. The field in the chain is excited via

near-field coupling by another loop antenna, located along the same axis, at the end of the disk chain. The receiving antenna is positioned at different positions along the chain by means of a PC-controlled high-precision near-field scanner. Both antennas are connected to the ports of a VNA, which took one transmission spectrum scan in a frequency band between 2.9 and 3.15 GHz for every spatial position of the receiving antenna. In such a setup the modulus of the transmission spectrum is proportional to the modulus of the radial component of the magnetic field in the near-field zone of the sample. The receiving antenna is positioned in steps of 0.5 mm. The normalized spectral and spatial distribution is shown in Fig. 5. The field profile for the selected frequency of 2.94 GHz is presented in the same figure in insets. The results of the numerical simulation for the radial component of the magnetic field distribution are also presented, showing good agreement with our experiment.

V. CONCLUSION

We have observed an accidental BIC in a one-dimensional periodic array composed of ceramic disks. In the experiment, we selectively excite a magnetic octupole mode with zero orbital angular momentum and measure the transmission spectrum using coaxially placed loop antennas. We extract the Q factor from the experimental data for the arrays with a varying number of disks and
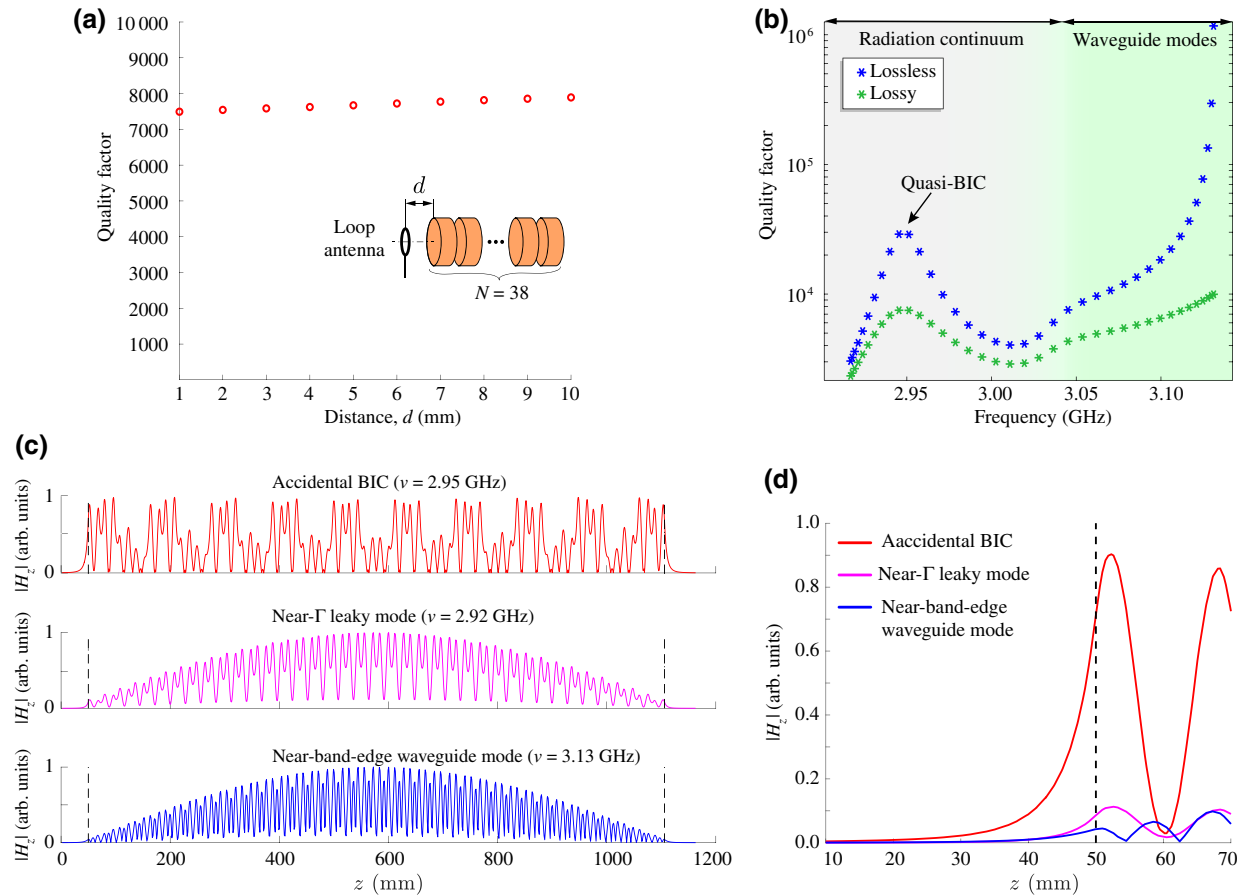
FIG. 6.   (a) Dependence of the loaded Q-factor on the distance between the loop antenna and the edge of the chain calculated for 38-disk chain accounting for losses in ceramics ($\tan\delta = 10^{-4}$). (b) Calculated dependence of Q-factor vs frequency of eigenmodes in a 38-disk chain. The blue and green stars correspond to lossless and lossy ($\tan\delta = 10^{-4}$) cases, respectively. (c) Distribution of the axial component of the magnetic field $|H_z|$ along the axis of the chain calculated for 38-disk chain for three eigenmodes. The vertical dashed lines show the boundary of the chain. Panel (d) shows the same distributions as in panel (a) but in the vicinity of the end of the chain. Each distribution is normalized to its the maximal value.

reveal a linear growth of the Q factor on the number of disks that is confirmed by our tight-binding model. For a certain ceramic with a material loss $\tan\delta = 1 \times 10^{-4}$, we find that radiation losses become negligible in comparison to material absorption when the number of disks is about 30 and, therefore, that the chain can be practically considered as infinite. The obtained results provide useful guidelines for practical implementations of structures with BICs that open up horizons for the development of radio-frequency and optical metadevices.

APPENDIX A: PARAMETERS OF THE SAMPLE

We consider an experimental sample consisting of a finite chain of at most 48 disks. Each disk is made of microwave ceramics with nominal dielectric permittivity $\varepsilon = 44$ and a tangent loss of $\tan\delta = 1 \times 10^{-4}$ in the frequency region 2–4 GHz. Each disk is 30 mm long and has a diameter of 30 mm. All the cylinders in the chain are aligned along the same axis and equidistant with a period of $L = 28$ mm. To ensure that all the disks are placed exactly at a specified distance from each other, a special holder made out of Styrofoam is fabricated on a CNC milling machine. The dielectric permittivity of Styrofoam is below 1.1, so its effective influence on the electromagnetic field distribution in a chain can be neglected. The

thickness of the holder is chosen to be enough to ensure that the near-field radiation of the sample does not interact with the table on which the sample is placed.

APPENDIX B: COUPLING BETWEEN THE CHAIN AND LOOP ANTENNA

It follows from coupled mode theory that the transmission spectrum through the resonance system in the single-resonance approximation is given by [57,58]

$$|S_{21}|^2 = \frac{\gamma_c^2}{(\omega - \omega_0)^2 + (\gamma_c + \gamma_{\text{rad}} + \gamma_{\text{NR}})^2}. \quad \text{(B1)}$$

Here, ω is the frequency of the incoming signal, ω_0 is the resonance frequency of the system, γ_c is the radiative loss arising due to the coupling with the port (loop antenna in our case), and γ_{rad} and γ_{NR} correspond to the radiative and nonradiative losses, respectively. In the considered chain of the ceramic disks, γ_{NR} is almost the same for all the modes as we work with a high-refractive-index ceramic providing almost perfect confinement of the electromagnetic field inside the disks.

One can see from Eq. (B1) that the transmission is maximal at the resonance when $\omega = \omega_0$. Moreover, the transmission is almost perfect when $\gamma_c \gg \gamma_{\text{rad}} + \gamma_{\text{NR}}$. Our simulation shows that we deal with a weak coupling regime when $\gamma_c \ll \gamma_{\text{rad}} + \gamma_{\text{NR}}$. Indeed, one can see from Fig. 6(a) that the loaded Q factor almost does not depend on the distance between the loop antenna and the edge of the chain and it is nearly the same as the Q factor of a bare chain. The weak coupling is also confirmed experimentally by the low absolute value of the $|S_{21}|^2$, which is about 10^{-3} [see Fig. 3(a)].

The radiative loss γ_{rad} however changes drastically within the considered frequency band. It is minimal for the quasi-BIC and waveguide modes [see Fig. 6(a)]. Thus, it seems that we should expect the maximal transmittance for these modes. However, γ_c depends on the overlap between the field of the antenna and the excited mode. As the field profiles are different for different modes, the coupling constant γ_c is also different.

To explain the fact that the transmission is minimal at the edges of the frequency band and maximal for the quasi-BIC, we analyze the field profiles for the quasi-BIC ($\nu = 2.94$ GHz), the waveguide mode at the band edge ($\nu = 3.13$ GHz), and the leaky mode near the Γ point ($\nu = 2.92$ GHz). In Figs. 6(c) and 6(d), we plot the absolute value of the axial component of the magnetic field $|H_z|$ since it is responsible for the magnetic flux through the loop antenna and, thus, the coupling efficiency. One can clearly see from Fig. 6(d) that outside the chain, $|H_z|$ decays faster for the waveguide mode at $\nu = 3.13$ GHz, and the leaky mode at $\nu = 2.92$ GHz rather than for the quasi-BIC. Therefore, the higher transmission at the frequencies near the quasi-BIC is explained by the low losses

$\gamma_{\text{rad}} + \gamma_{\text{NR}}$ (as we become closer to the critical coupling regime but still remain in the weak coupling regime) and more efficient coupling to the loop antenna in virtue of deeper penetration of the quasi-BIC field outside the chain.

---

[1] R. Meade, J. N. Winn, and J. Joannopoulos, *Photonic Crystals: Molding the Flow of Light* (Princeton University Press Princeton, NJ, 1995).

[2] S. G. Johnson, S. Fan, P. R. Villeneuve, J. D. Joannopoulos, and L. A. Kolodziejski, Guided modes in photonic crystal slabs, Phys. Rev. B **60**, 5751 (1999).

[3] P. Paddon and J. F. Young, Two-dimensional vector-coupled-mode theory for textured planar waveguides, Phys. Rev. B **61**, 2090 (2000).

[4] E. N. Bulgakov and A. F. Sadreev, Bound states in the continuum in photonic waveguides inspired by defects, Phys. Rev. B **78**, 075105 (2008).

[5] D. C. Marinica, A. G. Borisov, and S. V. Shabanov, Bound States in the Continuum in Photonics, Phys. Rev. Lett. **100**, 183902 (2008).

[6] J. von Neumann and E. P. Wigner, Über merkwürdige diskrete eigenwerte, Z. Physik **30**, 465 (1929).

[7] C. W. Hsu, B. Zhen, A. D. Stone, J. D. Joannopoulos, and M. Soljačić, Bound states in the continuum, Nat. Rev. Mater. **1**, 1 (2016).

[8] F. Monticone and A. Alu, Embedded Photonic Eigenvalues in 3d Nanostructures, Phys. Rev. Lett. **112**, 213903 (2014).

[9] Z. F. Sadrieva, M. A. Belyakov, M. A. Balezin, P. V. Kapitanova, E. A. Nenasheva, A. F. Sadreev, and A. A. Bogdanov, Experimental observation of a symmetry-protected bound state in the continuum in a chain of dielectric disks, Phys. Rev. A **99**, 053804 (2019).

[10] A. Taghizadeh and I.-S. Chung, Quasi bound states in the continuum with few unit cells of photonic crystal slab, Appl. Phys. Lett. **111**, 031114 (2017).

[11] G. S. Blaustein, M. I. Gozman, O. Samoylova, I. Y. Polishchuk, and A. L. Burin, Guiding optical modes in chains of dielectric particles, Opt. Express **15**, 17380 (2007).

[12] E. N. Bulgakov and D. N. Maksimov, Light enhancement by quasi-bound states in the continuum in dielectric arrays, Opt. Express **25**, 14134 (2017).

[13] L. Ni, J. Jin, C. Peng, and Z. Li, Analytical and statistical investigation on structural fluctuations induced radiation in photonic crystal slabs, Opt. Express **25**, 5580 (2017).

[14] J. Jin, X. Yin, L. Ni, M. Soljačić, B. Zhen, and C. Peng, Topologically enabled ultrahigh-q guided resonances robust to out-of-plane scattering, Nature **574**, 501 (2019).

[15] C. W. Hsu, B. Zhen, J. Lee, S.-L. Chua, S. G. Johnson, J. D. Joannopoulos, and M. Soljačić, Observation of trapped light within the radiation continuum, Nature **499**, 188 (2013).

[16] Z. F. Sadrieva, I. S. Sinev, K. L. Koshelev, A. Samusev, I. V. Iorsh, O. Takayama, R. Malureanu, A. A. Bogdanov, and A. V. Lavrinenko, Transition from optical bound states in the continuum to leaky resonances: Role of substrate and roughness, ACS Photonics **4**, 723 (2017).

[17] K. Koshelev, S. Lepeshov, M. Liu, A. Bogdanov, and Y. Kivshar, Asymmetric Metasurfaces with High-Q

Resonances Governed by Bound States in the Continuum, Phys. Rev. Lett. **121**, 193903 (2018).

[18] Z. Hu, L. Yuan, and Y. Y. Lu, Bound states with complex frequencies near the continuum on lossy periodic structures, Phys. Rev. A **101**, 013806 (2020).

[19] A. Kodigala, T. Lepetit, Q. Gu, B. Bahari, Y. Fainman, and B. Kanté, Lasing action from photonic bound states in continuum, Nat. Publishing Group **541**, 196 (2017).

[20] S. T. Ha, Y. H. Fu, N. K. Emani, Z. Pan, R. M. Bakker, R. Paniagua-Domínguez, and A. I. Kuznetsov, Directional lasing in resonant semiconductor nanoantenna arrays, Nat. Nanotechnol. **13**, 1042 (2018).

[21] S. Kim, K.-H. Kim, and J. F. Cahoon, Optical Bound States in the Continuum with Nanowire Geometric Superlattices, Phys. Rev. Lett. **122**, 187402 (2019).

[22] X. Gao, B. Zhen, M. Soljacic, H. Chen, and C. W. Hsu, Bound states in the continuum in fiber bragg gratings, ACS Photonics **6**, 2996 (2019).

[23] S. Romano, S. Torino, G. Coppola, S. Cabrini, and V. Mocella, in *Optical Sensors 2017* (International Society for Optics and Photonics, 2017), Vol. 10231, p. 102312J.

[24] Y. Liu, W. Zhou, and Y. Sun, Optical refractive index sensing based on high-q bound states in the continuum in free-space coupled photonic crystal slabs, Sensors **17**, 1861 (2017).

[25] S. Romano, G. Zito, S. Managò, G. Calafiore, E. Penzo, S. Cabrini, A. C. De Luca, and V. Mocella, Surface-enhanced raman and fluorescence spectroscopy with an all-dielectric metasurface, J. Phys. Chem. C **122**, 19738 (2018).

[26] K. Koshelev, Y. Tang, K. Li, D.-Y. Choi, G. Li, and Y. Kivshar, Nonlinear metasurfaces governed by bound states in the continuum, ACS Photonics **6**, 1639 (2019).

[27] J. M. Foley, S. M. Young, and J. D. Phillips, Symmetry-protected mode coupling near normal incidence for narrow-band transmission filtering in a dielectric grating, Phys. Rev. B **89**, 165111 (2014).

[28] X. Cui, H. Tian, Y. Du, G. Shi, and Z. Zhou, Normal incidence filters using symmetry-protected modes in dielectric subwavelength gratings, Sci. Rep. **6**, 1 (2016).

[29] L. L. Doskolovich, E. A. Bezus, and D. A. Bykov, Integrated flat-top reflection filters operating near bound states in the continuum, Photonics Res. **7**, 1314 (2019).

[30] K. L. Koshelev, S. K. Sychev, Z. F. Sadrieva, A. A. Bogdanov, and I. V. Iorsh, Strong coupling between excitons in transition metal dichalcogenides and optical bound states in the continuum, Phys. Rev. B **98**, 161113(R) (2018).

[31] V. Kravtsov, E. Khestanova, F. A. Benimetskiy, T. Ivanova, A. K. Samusev, I. S. Sinev, D. Pidgayko, A. M. Mozharov, I. S. Mukhin, and M. S. Lozhkin *et al.*, Nonlinear polaritons in a monolayer semiconductor coupled to optical bound states in the continuum, Light Sci. Appl. **9**, 1 (2020).

[32] J. Yoon, S. Song, and R. Magnusson, Critical field enhancement of asymptotic optical bound states in the continuum, Sci. Rep. **5**, 18301 (2015).

[33] V. Mocella and S. Romano, Giant field enhancement in photonic resonant lattices, Phys. Rev. B **92**, 155117 (2015).

[34] M. Zhang and X. Zhang, Ultrasensitive optical absorption in graphene based on bound states in the continuum, Sci. Rep. **5**, 8266 (2015).

[35] R. Magnusson and S. Wang, New principle for optical filters, Appl. Phys. Lett. **61**, 1022 (1992).

[36] T. Wang and S. Zhang, Large enhancement of second harmonic generation from transition-metal dichalcogenide monolayer on grating near bound states in the continuum, Opt. Express **26**, 322 (2018).

[37] T. Wang and X. Zhang, Improved third-order nonlinear effect in graphene based on bound states in the continuum, Photonics Res. **5**, 629 (2017).

[38] J. Ramos and P. Orellana, Bound states in the continuum and spin filter in quantum-dot molecules, Phys. B: Condens. Matter **455**, 66 (2014).

[39] H. M. Doeleman, F. Monticone, W. den Hollander, A. Alù, and A. F. Koenderink, Experimental observation of a polarization vortex at an optical bound state in the continuum, Nat. Photonics **12**, 397 (2018).

[40] B. Wang, W. Liu, M. Zhao, J. Wang, Y. Zhang, A. Chen, F. Guan, X. Liu, L. Shi, and J. Zi, Generating optical vortex beams by momentum-space polarization vortices centred at bound states in the continuum, Nat. Photonics **14**, 623 (2020).

[41] E. N. Bulgakov and A. F. Sadreev, Bloch bound states in the radiation continuum in a periodic array of dielectric rods, Phys. Rev. A **90**, 053801 (2014).

[42] E. N. Bulgakov and D. N. Maksimov, Light guiding above the light line in arrays of dielectric nanospheres, Opt. Lett. **41**, 3888 (2016).

[43] M. Padgett and R. Bowman, Tweezers with a twist, Nat. Photonics **5**, 343 (2011).

[44] A. Sit, F. Bouchard, R. Fickler, J. Gagnon-Bischoff, H. Larocque, K. Heshami, D. Elser, C. Peuntinger, K. Günthner, and B. Heim *et al.*, High-dimensional intracity quantum cryptography with structured photons, Optica **4**, 1006 (2017).

[45] E. N. Bulgakov and A. F. Sadreev, Light trapping above the light cone in a one-dimensional array of dielectric spheres, Phys. Rev. A **92**, 023816 (2015).

[46] E. N. Bulgakov and A. F. Sadreev, Bound states in the continuum with high orbital angular momentum in a dielectric rod with periodically modulated permittivity, Phys. Rev. A **96**, 013841 (2017).

[47] E. N. Bulgakov and A. F. Sadreev, Propagating bloch bound states with orbital angular momentum above the light line in the array of dielectric spheres, J. Opt. Soc. Am. A **34**, 949 (2017).

[48] E. Ivchenko and G. Pikus, Crystal Symmetry. In: *Superlattices and Other Heterostructures*. (Springer Series in Solid-State Sciences, Springer, Berlin, Heidelberg, 1995), Vol. 110.

[49] K. Sakoda, *Optical Properties of Photonic Crystals*, Springer series in optical sciences Vol. 80 (2001).

[50] Y. Yang, C. Peng, Y. Liang, Z. Li, and S. Noda, Analytical Perspective for Bound States in the Continuum in Photonic Crystal Slabs, Phys. Rev. Lett. **113**, 037401 (2014).

[51] Z. Sadrieva, K. Frizyuk, M. Petrov, Y. Kivshar, and A. Bogdanov, Multipolar origin of bound states in the continuum, Phys. Rev. B **100**, 115303 (2019).

[52] A. W. Snyder and J. Love, *Optical Waveguide Theory* (Springer Science & Business Media, NY, 2012).

[53] E. Bulgakov and A. Sadreev, Trapping of light with angular orbital momentum above the light cone, Adv. Electromagnetics **6**, 1 (2017).

[54] E. N. Bulgakov and A. F. Sadreev, High-q resonant modes in a finite array of dielectric particles, Phys. Rev. A **99**, 033851 (2019).

[55] L. Yuan and Y. Y. Lu, Strong resonances on periodic arrays of cylinders and optical bistability with weak incident waves, Phys. Rev. A **95**, 023834 (2017).

[56] E. N. Bulgakov and D. N. Maksimov, Topological Bound States in the Continuum in Arrays of Dielectric Spheres, Phys. Rev. Lett. **118**, 267401 (2017).

[57] S. Fan, W. Suh, and J. D. Joannopoulos, Temporal coupled-mode theory for the fano resonance in optical resonators, JOSA A **20**, 569 (2003).

[58] Q. Li, T. Wang, Y. Su, M. Yan, and M. Qiu, Coupled mode theory analysis of mode-splitting in coupled cavity system, Opt. Express **18**, 8367 (2010).